Mineralogy and Petrology (2002) 76: 39–62
DOI 10.1007/s00710-001-0184-x

Mineralogy and Petrology
Printed in Austria

Evidence for high silicic melt circulation and metasomatic events in the mantle beneath alkaline provinces: the Na–Fe-augitic green-core pyroxenes in the Tertiary alkali basalts of the Cantal massif (French Massif Central)

S. Pilet[1], **J. Hernandez**[1], and **B. Villemant**[2]

[1] Institute of Mineralogy and Geochemistry, University of Lausanne, Lausanne, Switzerland
[2] Laboratoire de Géochimie des systèmes volcaniques, Université P. et M. Curie, Paris, France

Received February 2, 2001; revised version accepted September 24, 2001
Published online July 31, 2002;

Summary

Na–Fe augitic green-core pyroxenes (hereafter called GCPX) are common in the silica-undersaturated basaltic rocks of many magmatic alkaline provinces. In the Cantal massif, green-core pyroxenes occur in nearly all the Supracantalian basalts (9.5 to 2 Ma), in contrast to the Infracantalian basalts (13 to 9.5 Ma) where they are rarely observed. An electron microprobe study demonstrates that the GCPX crystallized from evolved melts at intermediate to high pressures. Both Supra- and Infracantalian basalts show major and trace-element compositions similar to those of Ocean Island Basalts (OIB). However, the Supracantalian basalts exhibit an additional enrichment in Nb and Ta which we ascribe to a metasomatic event in the magma source. This enrichment could be related to the remobilization of metasomatic Ta and Nb-rich oxides located on grain boundaries in mantle peridotites (*Bodinier* et al., 1996). The hypothesis of the percolation of Si and K-rich metasomatic melts through the mantle is invoked to explain the deposition of these Ta–Nb oxides. On the basis of mineralogical and geochemical arguments, we suggest a relationship between these melts, the timing of the percolation and the formation of GCPX observed in Cantal basalts. We propose that GCPX crystallized in a melt differentiated by ''percolative fractional crystallization'' (PFC – *Harte* et al., 1993), a process which would account for the similar

major-element composition of the GCPX and pyroxenes observed in the phonolites of the Cantal massif. Amphibolitic siliceous metasomatic veins in peridotite xenoliths recently described by *Wulff-Pedersen* et al. (1999) contain augites similar in composition to the GCPX in Cantal basalts, in addition to Nb-rich oxides. This confirms the genetic relationship between metasomatic melts, GCPX and Nb-rich oxide parageneses. GCPX would therefore seem to be linked to a metasomatic event which took place both/either during and/or between the two main stages of basaltic outpouring, and is consequently contemporaneous with the volcanism. We suggest that this process may represent a common mechanism in many alkaline provinces, where asthenospheric upwelling generates silicic metasomatizing liquids by PFC. This metasomatic process is inferred to deposit accessory phases within the lithospheric mantle, a process followed by the subsequent inheritance of this metasomatic imprint by the younger basalts.

Introduction

Na–Fe augitic green cores (GCPX) are a frequent feature found within augitic clinopyroxenes of alkali basalts, basanites, nephelinites or leucitites. They have been described in many alkali basaltic provinces such as the French Massif Central (e.g. *Babkine* et al., 1968; *Hernandez*, 1971, 1973; *Wass*, 1979), the Eifel (*Huckenholz*, 1966; *Duda* and *Schmincke*, 1985 and references therein), Italian volcanic regions (*Civetta* et al., 1979; *Barton* et al., 1982), Hungary (*Dobosi* et al., 1992), the Canaries (*Frisch* and *Schmincke*, 1970), the Leucite Hills (USA) (*Barton* and *Bergen*, 1981), Uganda (*Lloyd*, 1981), Isla da Trinidade (*Greenwood*, 1998) and Morocco (*Rachdi* et al., 1985; *Ibhi*, 2000).

However, their origin is still a matter of debate. For instance, *Barton* and *van Bergen* (1981) concluded that the green pyroxenes from the Leucite Hills lava formed either during local mantle metasomatism or by crystallization of differentiated magmas of unknown origin. Since then, *Duda* and *Schmincke* (1985) have suggested that these pyroxenes crystallized in SiO_2-rich differentiated liquids during a high-pressure stage of differentiation near the mantle/crust boundary.

We carried out a study of the green pyroxenes in the basaltic rocks of the Cantal massif in the French Massif Central to test these contrasting hypotheses within a context of silica-undersaturated and -oversaturated alkaline series. The Cantal alkaline province displays a large spectrum of basaltic and intermediate compositions and, as has been suggested by *Liotard* et al. (1999), shows the existence of a metasomatized mantle directly below this province.

The Cantal massif

The Cantal massif is located in the French Massif Central, 150 km south of Clermont-Ferrand. With a volume of 2500 km^3 and a surface of approximately 5000 km^2, the Cantal massif is the largest Tertiary stratovolcano of the Tertiary-Quaternary volcanic province of western and central Europe. The main phase of magmatic activity between 13 and 2 Ma established the Cantal massif on a bulge of the Variscan granitic and metamorphic basement of the Massif Central.

Between 13 and 2 Ma, three main magmatic periods occurred (*Nehlig* et al., 2001). The first period (13 to 9.5 Ma) was characterized by the emission of scattered alkali basalt or basanite flows and the formation of strombolian cones. Differentiated

terms are missing from the beginning of the Cantal volcanic activity. During the second period (9.5 to 6.5 Ma), a complex stratovolcano, perhaps 3000–4000 m high, was formed by paroxysmal activity between 8.5 to 7.5 Ma. The corresponding lavas are essentially trachybasaltic to trachytic; at the end of this period, several phonolitic domes intruded along a SSE-NNW fault system. Pyroclastic events (*Platevoet* et al., 1999) and several debris avalanches (*Bourdier* et al., 1989; *Cantagrel*, 1995; *Schneider* and *Fischer*, 1998; *Reubi* and *Hernandez*, 2000) partially destroyed the stratovolcano and flattened its shape. The lavas which erupted during the last period (6.5 to 2 Ma) were again basaltic in composition and formed numerous dykes in the center of the massif as well as large lava flows (''planezes'') covering the foot of the volcano, except in its south-western part. The Ice Age and subsequent erosion put the final touch to the present landscape, with large valleys radiating from the center of a massif culminating at 1855 m (Plomb du Cantal).

Magmatic evolution

The Mont Dore, Chaîne des Puys and Cantal massifs show an association of SiO_2-saturated and SiO_2-undersaturated magma series (*Jung* and *Brousse*, 1962; *Brousse* et al., 1979; *Maury* and *Varet*, 1980).

The Cantal contains two mildly potassic alkaline series (Fig. 1). The undersaturated series is composed of basanites, tephrites and phonolites. The oversaturated

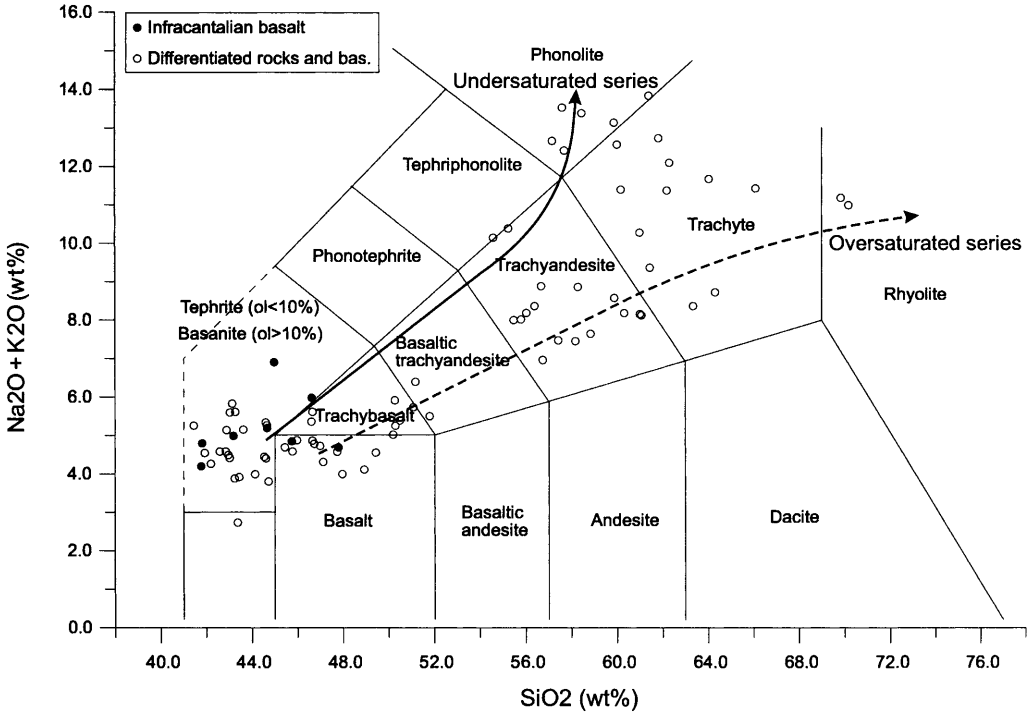

Fig. 1. Total alkalis vs silica diagram for the undersaturated and the oversaturated series of the Cantal basaltic province. Classification and nomenclature from *Le Maitre* et al. (1989). Data source from *Collomb* and *Pilet* (1996)

series includes trachybasalts, trachyandesites, trachytes and rhyolites. The SiO_2-undersaturated lavas are present in minor proportion compared to oversaturated rocks, with the exception of basanites, which are common.

Several hypotheses have been suggested to explain the existence of contrasted series and in particular the presence of differentiated SiO_2-oversaturated products, essentially suggested for the Mont Dore area but also used for the Cantal massif: 1) crustal contamination (*Brousse* et al., 1979); 2) hybridization of mantle- and crust-derived magmas (*Glangeaud* and *Letolle*, 1966); 3) fractional crystallization, particularly amphibole fractionation (*Maury*, 1976; *Maury* et al., 1980; *Villemant* et al., 1980; *Villemant*, 1985; *Collomb* and *Pilet*, 1996). More recently, *Downes* (1984) and *Wilson* et al. (1995) suggested that AFC processes may explain the evolution of the two series and, in particular, their isotopic (Sr, Nd) compositions. The origin of these two distinct differentiation series is determined mainly by the composition of the parental basaltic melts: basanitic melts leading to SiO_2-undersaturated series and alkali basaltic melts to SiO_2-oversaturated series.

The two main periods of basalt emission, from 13 to 9.5 Ma and from 9.5 to 2 Ma, are usually referred to as the Infracantalian and Supracantalian basalts respectively.

Mineralogy

Most of the Cantal lava flows are porphyritic with variable phenocryst contents (5 to 35%) (Fig. 2). The mineralogical composition of the Infracantalian and Supracantalian alkali basalts and basanites is similar.

Olivine shows variable compositions in basanites (Fo_{88-74} from the core to the rim) and alkali basalts (Fo_{84-70}) whereas it is absent from basaltic trachyandesites and more differentiated lava flows.

Clinopyroxene is present as phenocrysts and in the groundmass of all the rocks from the SiO_2-undersaturated series, but is not observed in trachytes with a poor alkali content nor in rhyolites. Clinopyroxene is more abundant in basanites than in alkali basalts. In mafic rocks, feldspar phenocrysts (An_{64-34}) are present only in alkali basalts. Amphibole (kaersutite) is present from basaltic trachyandesites to phonolites and trachytes, but not in rhyolites. *Maury* (1976), *Maury* et al. (1980), *Villemant* et al. (1981) and *Wilson* et al. (1995) emphasized the role of this mineral in the differentiation process of the two series. More SiO_2-undersaturated rocks contain feldspathoïds (nepheline or leucite in the groundmass of basanites, hauyne, sodalite or nosean as phenocrysts in tephrites and phonolites). Fe–Ti oxides (magnetite and/or ilmenite) are observed as microphenocrysts and microcrysts throughout the basalt series. Apatite and zircon are present in trachyandesites, phonolites and trachytes, but are absent in rhyolites. The same feature also applies to titanite, which sometimes forms large phenocrysts in trachyandesites and phonolites, but is absent from alkali-poor trachytes and rhyolites.

GCPX are common in Supracantalian basalts and basanites (Plate 1, photograph 1) and exceptionally occur in Miocene Infracantalian basalts. We observed different habits of crystals (Plate 1, photographs 1, 2 and 3), where three main zones can usually be distinguished. The core zone, dark to light green in color, is usually resorbed and surrounded by zoned inner and outer rims. The colorless

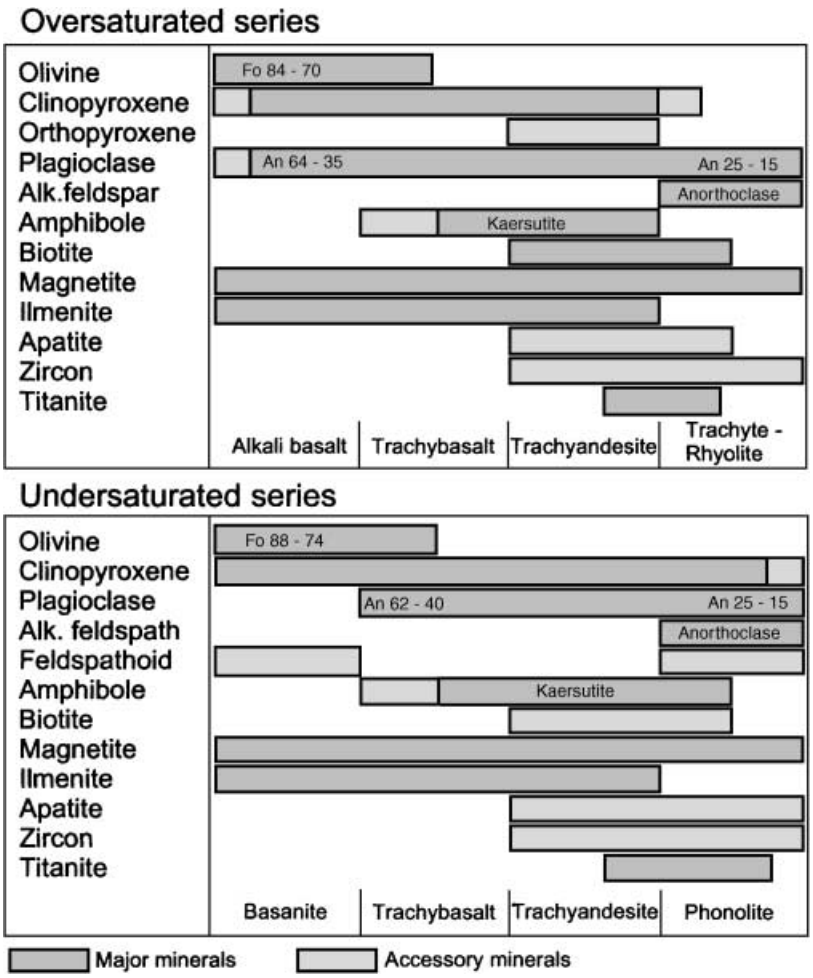

Fig. 2. Phenocryst mineralogy of the oversaturated and the undersaturated series of the Cantal basaltic province

weakly zoned inner rim evolves into a zoned brownish outer rim. These last two zones, which occur in all clinopyroxene phenocrysts, are comagmatic. The colorless inner rim is Cr-rich, whereas the brownish rim corresponds to the Ti-augite chemical composition of the groundmass clinopyroxenes. The shape, color and zoning of the cores are highly variable even within a single sample. Hourglass zoning may be present (Plate 1, photograph 2), demonstrating a fast crystallization rate for some of the cores. Most of the cores show a resorption step before the crystallization of the colorless inner rim zone. Apatite, oxides and very occasionally glass inclusions are found (Plate 1, photograph 2) in green cores. Finally, in some rocks, the GCPX can form polycrystalline aggregates (Plate 1, photograph 3).

We carried out a systematic microprobe study of the pyroxenes in the basalts and the other lavas to determine the origin of the GCPX (Table 1). All analyzed pyroxenes have a QUAD composition according to the pyroxene classification of *Morimoto* et al. (1988). The pyroxenes of basalts and basanites show limited variation in composition, from $Wo_{42.4}En_{46.9}Fs_{10.7}$ to $Wo_{46.7}En_{38.8}Fs_{14.6}$ in the

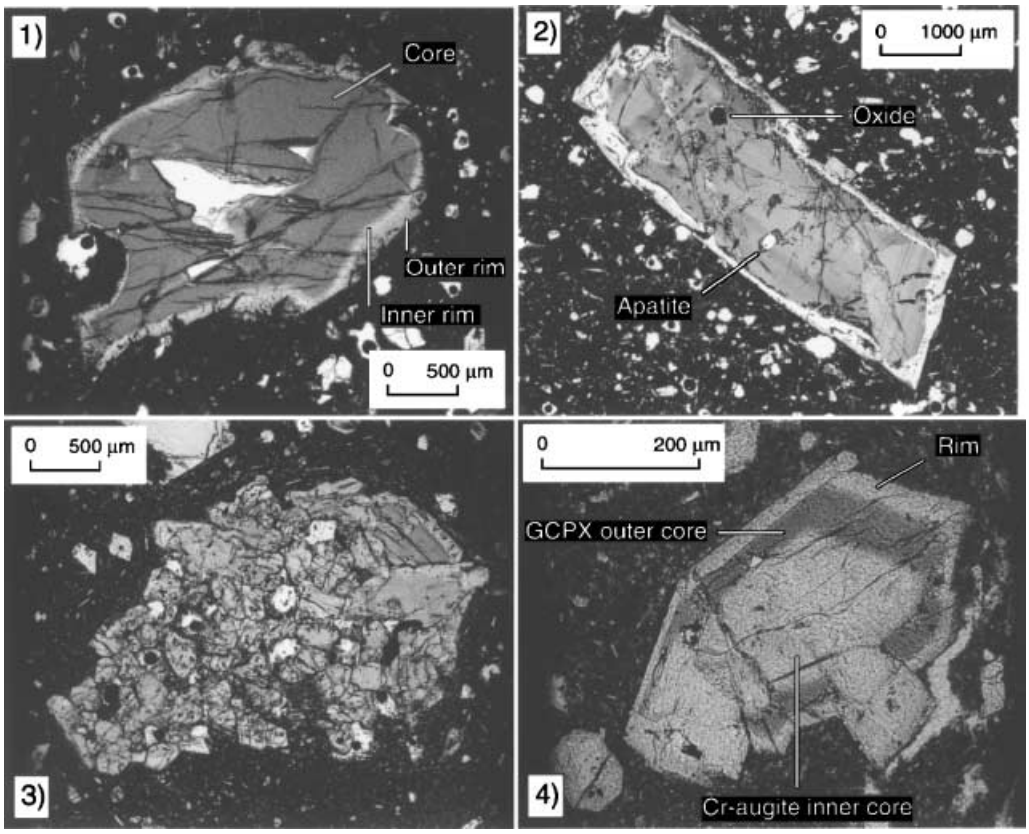

Plate 1. (**1**) Typical green-core pyroxene with light Cr-augite inner rim and brownish Ti-augite rim. (**2**) Green-core pyroxene with apatite, oxide and glass inclusions. (**3**) Green-core CPX cumulate with common light rim. (**4**) Clinopyroxene with composite core: Cr-augite inner core, GCPX outer core, light augitic rim and outer Ti-augite rim. Note the growth of two Cr-augite cores before crystallization of outer GCPX core. This growth association exclude in our sense the possibility of crystallization of the inner core after dissolution of a previous GCPX (see text for explanation)

basalts and $Wo_{45.9}En_{42.3}Fs_{11.7}$ – $Wo_{50.7}En_{34.7}Fs_{14.6}$ in the basanites. The compositional variation of pyroxenes in phonolites occupies the range $Wo_{48}En_{33}Fs_{19}$ to $Wo_{45}En_{25}Fs_{30}$. The pyroxenes from the trachytes have a more restricted composition ($Wo_{43.9}En_{42.9}Fs_{13.2}$ to $Wo_{46.2}En_{37.2}Fs_{16.6}$). The GCPX show the same range of compositions as the phonolitic pyroxenes. This feature can be noted in the Fe(2+)–Na diagram (Fig. 3). In contrast, the pyroxenes from trachytes display lower Na concentrations than the pyroxenes from phonolites and GCPX. Composition ranges for the other elements (Mg, Al, Ca, Mn, K ...) are also similar in pyroxenes from phonolites and GCPX, except for the total Al/Ti ratio (Fig. 4).

Thompson (1974) demonstrated that the total Al/Ti ratio in clinopyroxene is correlated to the crystallization pressure. Compared to the other pyroxenes, the GCPX of Cantal lavas are characterized by a higher and more variable Al/Ti ratio (Fig. 4). According to *Thompson's* (1974) experimental work on this ratio, the compositions of pyroxenes from basalts to phonolites correspond to crystallization

Table 1. *Representative microprobe analyses of green-core pyroxene, mantle and rim composition from Infracantalian and Supracantalian basalts. Analyses Pav 13 CPX from* Wulff-Pedersen *et al. (1999). Analytical condition: acceleration potential 15 Kv, beam current 30 nA; analytical time: 15 sec for Si, Mg and Ca; 30 sec for Ti, Al, Cr, Fe, Mn and Na*

No analyses	Supracantalian rocks							Infracantalian rocks			
Type of rock	Green-core ac2,5,44 Basanite	Green-core ac3,1e,54 Alk. basalt	Green-core SP4 mb13_3 Basanite	Green-core ac2,2a,21 Basanite	Green-core SP31c9_1 Basanite	Mantle ac3,4a,118 Alk. basalt	Rim ac3,1e,51 Alk. basalt	Green-core M10 min9_1 Basanite	Green-core M10 min16_3 Basanite	Pav 13 CPX	Pav 13 CPX
SiO_2	48.82	49.21	48.02	48.14	46.14	50.72	44.72	46.85	43.35	48.37	47.77
TiO_2	0.81	1.29	1.48	0.65	1.35	1.24	3.63	1.22	1.79	1.36	1.26
Al_2O_3	4.88	4.92	5.51	4.38	8.85	3.50	7.76	6.47	9.15	4.99	4.75
Cr_2O_3	0.01	0.00	0.02	0.00	0.08	0.53	0.17	0.02	0.05		
Fe_2O_3	6.41	4.54	5.87	8.74	4.91	2.01	3.90	7.98	8.70	5.54	6.03
FeO	6.50	3.71	5.00	8.49	3.91	3.55	4.51	6.49	6.86	5.88	4.98
MnO	0.56	0.20	0.23	1.24	0.20	0.10	0.12	0.50	0.45	0.55	0.46
MgO	9.29	12.83	10.50	6.75	11.39	15.49	11.84	7.75	6.69	9.96	9.99
CaO	20.71	22.32	21.61	19.92	21.76	22.38	22.45	20.54	21.48	22.19	21.82
Na_2O	1.93	1.00	1.53	2.34	0.88	0.39	0.48	2.16	1.44	1.39	1.52
Total	99.92	100.02	99.77	100.65	99.47	99.91	99.58	99.98	99.96	100.23	98.58
End-Members											
Acmite	14.19	7.18	11.20	17.38	6.41	2.82	3.52	15.94	10.77	10.16	11.27
Ca–$CrFe^{3+}$ tsch.	2.05	2.77	2.75	3.90	3.83	2.15	4.01	3.49	7.29	2.77	3.05
Ca–Ti tsch.	2.30	3.59	4.20	1.88	3.81	3.44	10.29	3.50	5.19	3.85	3.62
Ca-tsch.	8.59	7.17	8.03	8.00	15.72	4.15	6.93	11.01	15.56	7.23	7.08
Wollastonite	35.51	37.67	36.11	33.97	31.98	39.29	34.69	32.91	30.25	37.87	37.81
Enstatite	26.19	35.54	29.48	19.27	31.79	42.52	33.24	22.00	19.18	27.97	28.46
Ferrosilite	11.17	6.08	8.24	15.61	6.44	5.62	7.30	11.14	11.76	10.14	8.71
Mg#	0.61	0.77	0.68	0.45	0.73	0.85	0.74	0.55	0.48	0.66	0.67
Al/Ti	9.48	5.99	5.82	10.50	10.25	4.41	3.35	8.29	8.00	5.75	5.91

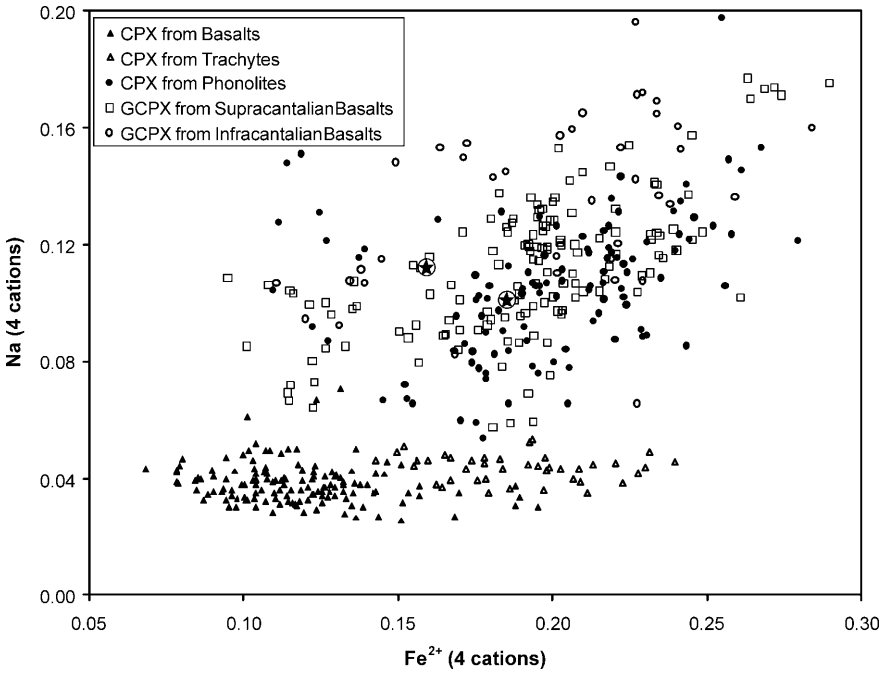

Fig. 3. Na vs Fe^{2+} diagram for representative Cantal pyroxenes, calculated with a structural formula on the basis of 4 cations. Stars: pyroxene analyses from *Wulff-Pedersen* et al. (1999). In all GCPX, the Fe^{3+} content is higher than the Na content, so Na is quantitatively used for the acmite component, whereas excess Fe^{3+} forms the Ca–CrFe^{3+} Tschermak molecule

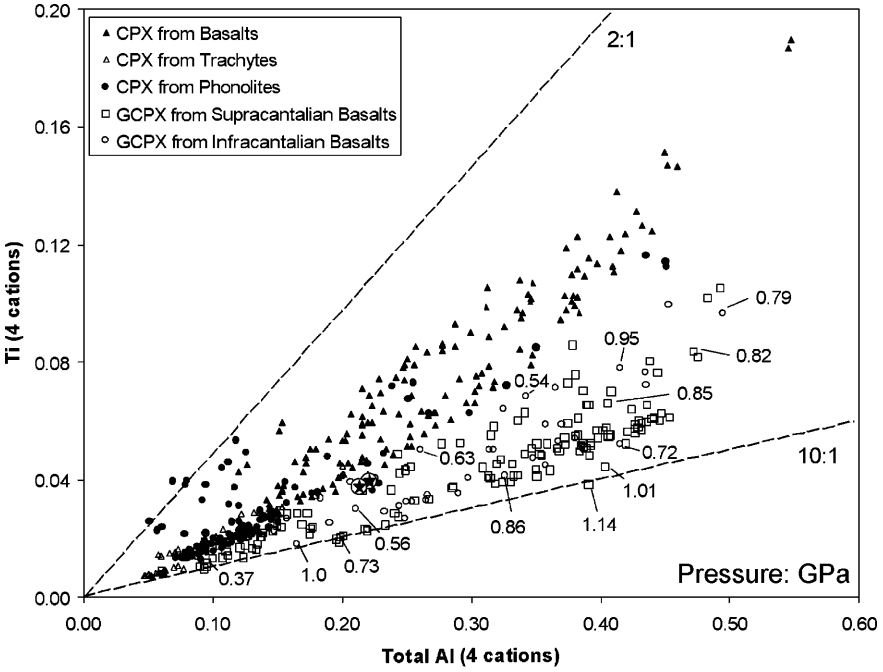

Fig. 4. Ti vs total Al Total diagram for representative Cantal pyroxenes, calculated with a structural formula on the basis of 4 cations. Numbers: minimum pressures of crystallization for green core pyroxene, see text for explanations

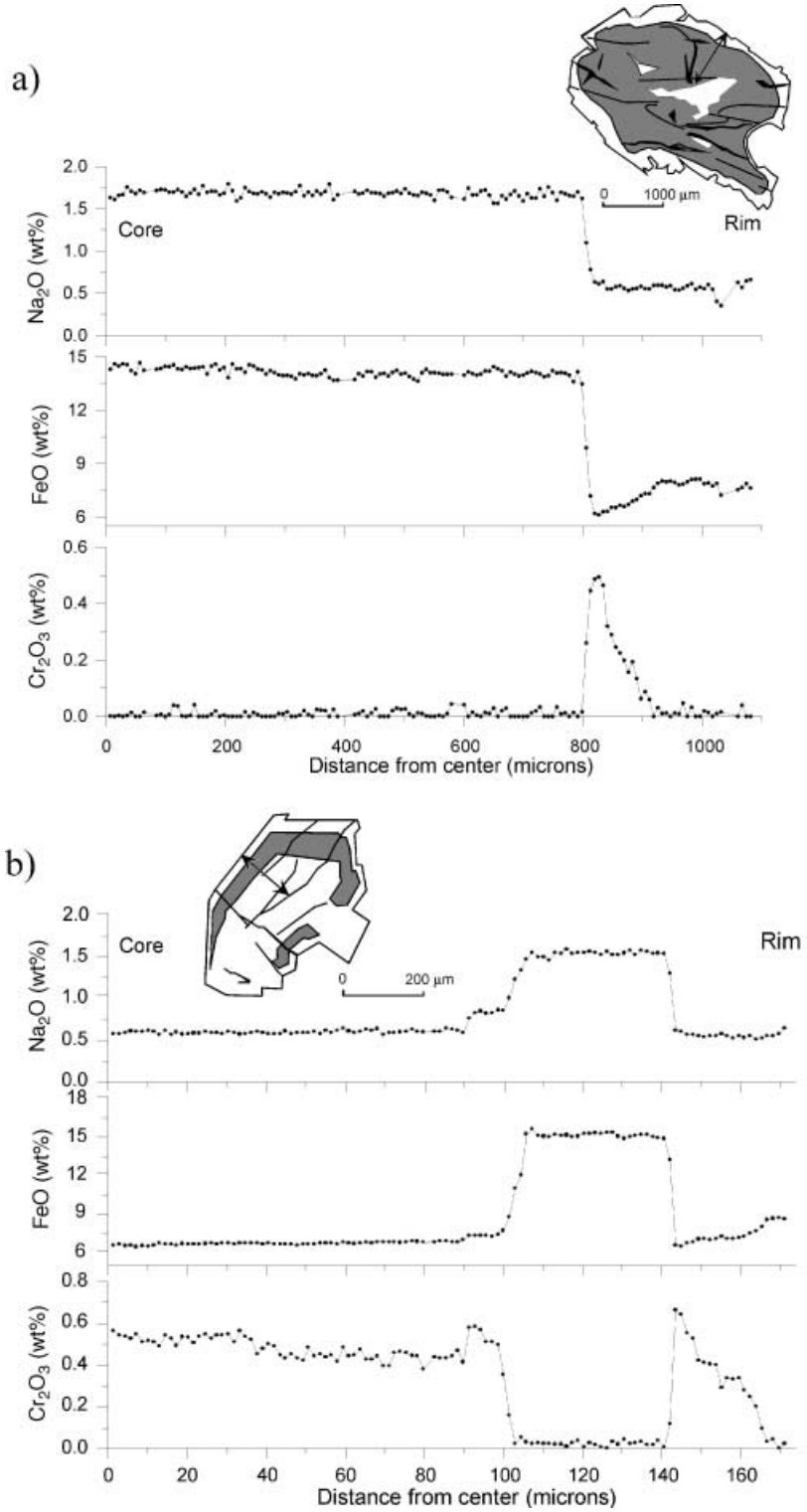

Fig. 5. **a** Typical line scan through a green-core pyroxene with lightly colored mantle and brownish rim. **b** Line scan through a clinopyroxene with composite core

pressures ranging from 0.2 to 0.3 GPa. We recalculated the crystallization pressures for GCPX using the clinopyroxene geobarometer of *Nimis* (1999). In order to calibrate the geobarometer, which is weakly temperature-sensitive, we estimated the minimum crystallization temperature of GCPX on the basis of the phonolitic pyroxene microcrystals under the assumption that they crystallize at $P \sim 1$ atm. Our estimate came to 1030–1050 °C. Using this temperature, we obtained pressures from 0.2 to 0.3 GPa for phonolite phenocrysts, which are in agreement with the Al/Ti ratios observed there. When applied to GCPX of the basalts, the barometer gives a range of pressures from 0.3 to 1.1 GPa, which are interpreted to be minimum values. These pressures correspond to crystallization depths for the GCPX ranging from the upper mantle condition to lithostatic pressures commonly observed in the intermediate continental crust, considering a Moho depth of 28–29 km (*Perrier* and *Ruegg*, 1974).

We performed more than 20 compositional line scans through GCPX; a representative profile is shown in Fig. 5a. The core shows a constant Al/Ti ratio and the Na and Fe contents are stable. The inner rim is characterized by an increase of the Cr content, demonstrating the primitive nature of the basaltic liquid within which this pyroxene zone has grown. The transition from the inner rim to the outer rim corresponds to a compositional evolution that is consistent with crystallization under decreasing pressures with increasing Al, Ti and Fe contents and decreasing Si, Mg contents and Al/Ti ratios. This evolution is in accordance with the evolution of the inner and outer rims in a basaltic liquid by fractional crystallization during its ascent. On the other hand, the rounded shape of the green cores provides evidence for the existence of a resorption stage before the crystallization of the inner rim: they could therefore be interpreted as xenocrysts.

In contrast, the formation of composite cores (Plate 1, photograph 4) with intergrowth of euhedral GCPX and augite could be explained by mixing between a basaltic liquid within which the Mg- and Cr-rich core crystallized (Fig. 5b) and a ''phonolitic'' liquid from which the green zone crystallized. Indeed, this latter zone has the same composition as the xenocrystic green cores. Subsequently, the outer rim crystallized either in the same basaltic liquid or within a new pulse of primitive basaltic liquid. Different formation modes are needed to explain the two different types of associations. However, both require the presence of a liquid of phonolitic composition.

Geochemistry

Methods

We analyzed major and trace elements in 11 Infracantalian basalts, 22 Supracantalian basalts and 18 differentiated rocks (Fig. 1). Trace elements were analyzed by INAA at the P. Süe laboratory (Saclay, France). We carried out complementary analyses for REE on selected samples by ICPMS (X-Ral, Canada) and for Nb, Zr, Y and Pb by applying a high-precision X-ray fluorescence technique (CAM, Lausanne). In addition, we analyzed 11 Infracantalian basalts by X-ray fluorescence, and five by ICPMS for REE.

Results

Table 2 shows representative analyses of eight Infracantalian and Supracantalian basalts and basanites and two phonolites. Basalts and basanites (Fig. 1) show a wide range of SiO_2 contents ($\sim$40 to 51 wt%) within a restricted range of alkali content ($\sim$4 to 6 wt%). Figure 6a shows primitive mantle-normalized patterns for typical alkali basalts (37, 39) and basanites (31, 32, 9) from the Supracantalian period. The similarity between the patterns of basanites and alkali basalts suggests a common mantle source for these rocks. The variation of their incompatible element contents might be explained by a smaller degree of partial melting for basanites than for alkali basalts. Furthermore, the distribution of the trace elements from basanites and alkali basalts shows a strong similarity with OIB patterns [range of OIB composition from the compilation of *Wedepohl* and *Baumann* (1999 and references therein)]. These authors demonstrate the existence of compositional similarities between Cenozoic volcanic rocks in Germany (similar to the lavas of the French Massif Central) and OIB. The similarity to OIB compositions is also observed in the Infracantalian basalts (Fig. 6b) and their higher content of incompatible elements (Th, La, Ce, ...) compared to the Supracantalian basalts might reflect an even lower degree of partial melting within a similar source.

However, the Th–Nb diagram (Fig. 7a) shows contrasting behavior between the Infracantalian and Supracantalian basalts. The former show a relatively straight linear trend, resulting from limited variation of the Nb/Th ratio in these rocks (Fig. 7b), in contrast to the latter, which show a clear enrichment in Nb. Considering that Nb and Th are both highly incompatible elements, a linear trend in the Th–Nb diagram is consistent with a variation in the degree of partial melting of a normal mantle (corresponding to a fertile spinel or garnet lherzolite). Furthermore, the Nb/Th ratio of Infracantalian basalts is relatively similar to that of representative OIB analyses performed by *Hémond* et al. (1994), *Chauvel* et al. (1992), and *Allègre* et al. (1995) (Fig. 7a).

The Supracantalian basalts do not show a straight linear trend in the Nb–Th diagram. This results from a change of the Nb/Th ratio from basalts to basanites (Fig. 7b). Other incompatible elements (La, Ce, Th, ...) do not show contrasting behavior between Infra- and Supracantalian rocks (Fig. 7c), except for Ta, with variations similar to Nb. This is illustrated in the Th–Ta/Th diagram (Fig. 8a) which shows a clear variation from basalts to basanites for Supracantalian rocks.

We examined various hypotheses to explain this decrease of the (Ta, Nb)/Th ratio from basalts to basanites in Supracantalian lavas:

Fractional crystallization

The range of variation of the Ni content in the selected basalts is 260 to 150 ppm. Considering that Nb, Ta and Th are all highly incompatible (*Lemarchand* et al., 1987; *Sun* and *McDonough*, 1989), the fractional crystallization of olivine and/or pyroxene, in the above range of Ni content, cannot account for a large variation of the Nb, Ta and Th content in the residual liquid and for a variation of the Nb/Th or Ta/Th ratios.

Table 2. *Representative analyses of Infracantalian basalts, Supracantalian basalts and phonolites. Numbers in italics: XRF analyses, underlined numbers: INAA analyses. Major and trace elements by XRF analyses at Centre d'Analyse Minérale (CAM) University of Lausanne. INAA analyses at P. Süe Laboratory, Saclay, France. REE analyses by ICP-MS at Xral Laboratories, Canada. For INAA, uncertainties in % indicated in italics in the second column. For XRF and ICP-MS analyses, uncertainties varied with the concentration, and only the detection limit is indicated (second column)*

Major elements (XRF)		Supracantalian Basalts						Infracantalian Basalts			
		31 basanite	**32** basanite	**37** Alk. basalt	**39** Alk. basalt	**48** phonolite	**49** phonolite	**M3** Alk. basalt	**M4** basanite	**M7** basanite	**M8** basanite
SiO_2 (wt%)		41.44	43.03	46.97	48.91	57.59	57.68	41.78	44.65	41.82	44.96
TiO_2		3.23	3.33	2.45	2.20	0.22	0.48	2.61	2.84	2.65	2.41
Al_2O_3		13.05	12.38	14.03	14.09	20.47	20.10	12.67	13.69	11.94	13.86
Fe_2O_3		6.36	4.67	2.83	3.32	2.19	0.98	7.34	7.18	4.50	5.40
FeO		6.15	6.65	7.94	7.21	0.00	1.71	5.12	5.01	6.99	4.30
MnO		0.21	0.17	0.17	0.15	0.21	0.18	0.20	0.17	0.19	0.18
MgO		10.58	9.90	9.76	9.82	0.15	0.57	10.58	10.39	12.93	7.42
CaO		11.58	9.70	9.75	8.91	0.87	2.37	10.95	9.92	10.60	10.16
Na_2O		3.58	2.85	3.44	3.02	7.92	6.74	2.21	3.52	2.52	4.77
K_2O		1.67	2.74	1.29	1.09	5.61	5.67	1.99	1.67	2.27	2.14
P_2O_5		1.05	1.14	0.61	0.42	0.02	0.08	1.01	0.79	0.99	0.91
LOI		0.41	2.02	0.39	0.73	3.97	2.52	3.23	0.20	2.38	2.97
Total		99.31	98.58	99.69	99.93	99.22	99.07	99.76	100.07	99.87	99.51
Trace elements (INAA)											
Sc (ppm)	*2.3*	26.0	26.0	26.4	24.3	0.7	2.0				
Cr	*2.5*	280	235	302	324	11	17	*328*	*257*	*487*	*256*
Co	*3.3*	50.0	50.5	51.6	50.0	0.7	2.8				
Ni	*1.9*	194	213	211	261	0	3	*241*	*223*	*359*	*133*
Rb	*3.4*	55.3	70.4	28.8	21.8	297.3	199.7	*48.2*	*41.7*	*45.2*	*77.2*
Sr	*2.6*	940	1027	716	625	37	246	*940*	*737*	*929*	*1359*
Sb	*23.1*	0.15	0.13	0.07	0.03	1.16	0.68				
Cs	*2.5*	0.64	0.69	0.37	0.29	7.41	4.35				
Ba	–	621.7	740.0	461.8	356.9	27.1	393.1	*741*	*531*	*761*	*963*
La	*2.7*	76.6	77.4	45.9	32.8	97.0	66.6	*79*	*48*	*75*	*134*

(*continued*)

Table 2 (*continued*)

Major elements (XRF)		Supracantalian Basalts						Infracantalian Basalts			
		31 basanite	**32** basanite	**37** Alk. basalt	**39** Alk. basalt	**48** phonolite	**49** phonolite	**M3** Alk. basalt	**M4** basanite	**M7** basanite	**M8** basanite
Ce	*5.9*	150.2	146.4	89.5	64.7	109.7	84.2	*137*	*86*	*132*	*201*
Sm	*2.5*	14.0	12.8	9.3	7.6	3.4	1.4				
Tb	*2.3*	1.20	1.02	0.90	0.75	0.15	0.23				
Yb	*4.4*	2.3	1.9	1.9	1.6	2.0	1.5				
Hf	*5.17*	7.9	8.7	5.8	5.0	20.9	14.0				
Ta	*1.7*	8.3	7.2	5.6	4.1	3.1	2.5				
Th	*2.9*	9.0	9.0	5.5	3.4	47.1	25.7				
Trace elements (XRF)											
Y (ppm)	0.14	33.7	27.7	26.2	23.3	9.3	9.2	28.2	24.8	28.3	27.9
Zr	0.14	387	418	301	236	1405	986	335	273	346	462
Nb	0.12	114.3	110.9	83.2	62.2	193	110.5	100.4	68.5	101.6	144.9
Pb	0.5	3	4	2	2	23	14	4	2	3	8
REE (ICP-MS)											
La (ppm)	0.1	79.3	74.1	43.1	33.0			70.4	45.5	67.2	146
Ce	0.1	163	145	83.4	67.1			142	93.4	134	235
Pr	0.2	17.2	15.3	9.2	7.5			15.0	10.3	14.4	20.4
Nd	0.1	80.3	69.1	43.3	36.1	14.1	22.5	67.0	48.4	64.9	78.4
Sm	0.1	14.4	12.2	8.7	7.5			11.9	9.5	11.4	12.5
Eu	0.05	4.04	3.41	2.72	2.32			3.64	2.97	3.37	3.56
Gd	0.1	12.4	10.2	8.8	6.7			11.1	9	10.5	9.2
Tb	0.1	1.3	1.1	1.0	0.9			1.2	1	1.1	1.4
Dy	0.1	8.1	7.0	6.0	5.3			7.5	6.4	6.9	6.7
Ho	0.05	1.29	1.04	0.95	0.87			1.13	0.94	1.09	1.28
Er	0.1	3.8	3.0	2.8	2.4			3.3	2.8	3.2	2.8
Tm	0.1	0.4	0.3	0.3	0.3			0.4	0.3	0.4	0.4
Yb	0.1	2.9	2.2	2.2	1.9			2.4	2.1	2.3	2.3
Lu	0.05	0.37	0.27	0.27	0.27			0.3	0.27	0.31	0.41
U	0.1	2.7	2.6	1.6	0.9	15	8	2.8	1.6	2.5	5.3
Th	0.1	10.5	10	6.1	4.1			9.8	6.3	9.4	18.0

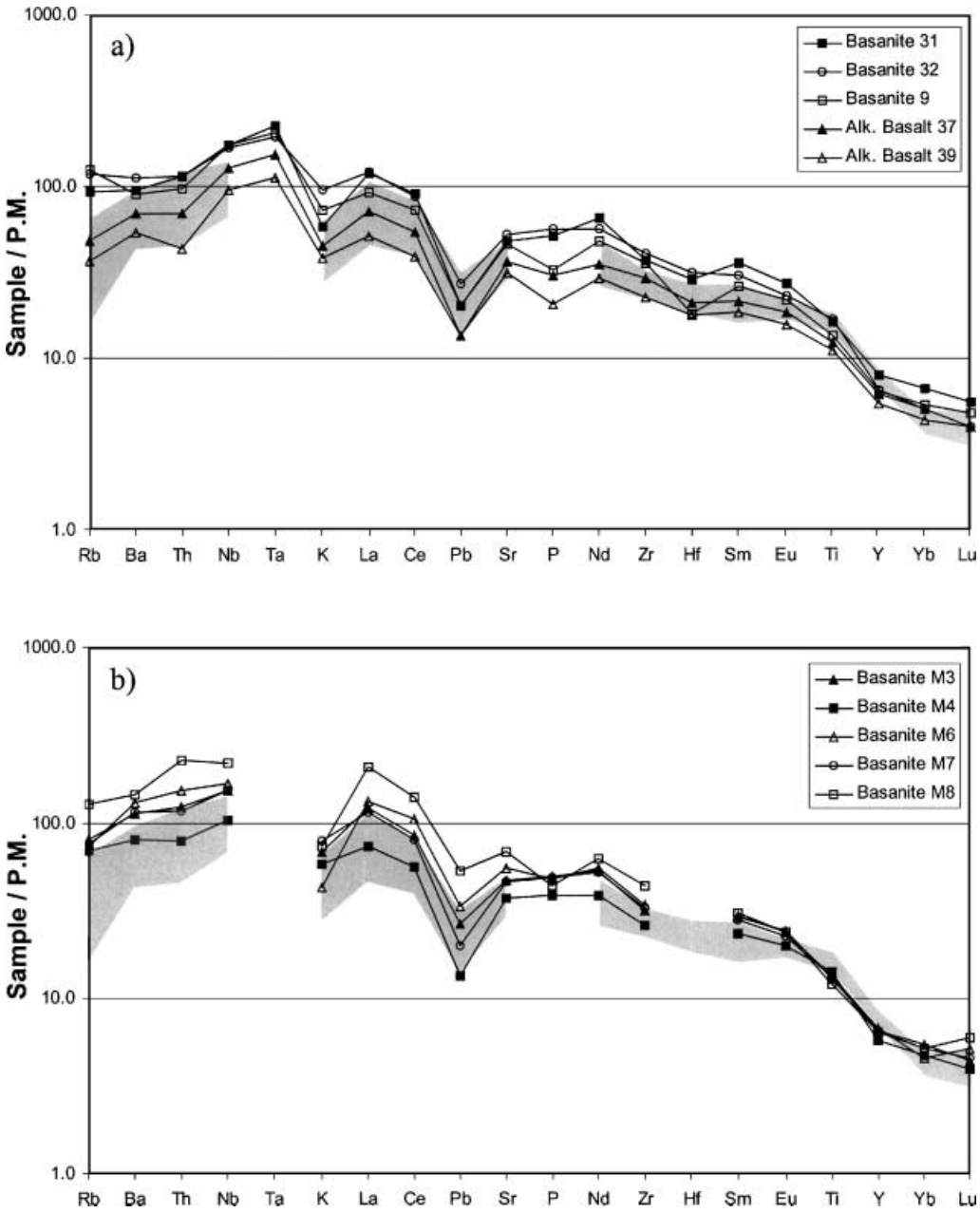

Fig. 6. Primitive mantle normalized trace element variation diagrams for **a** Supracantalian basalts, **b** Infracantalian basalts. Normalization values from *McDonough* (1998)

Variations of the partial degree of melting

To explain the observed variation of the Ta/Th ratio during partial melting, the D_{Ta}/D_{Th} ratio should be around 10 (Fig. 8a). Ta and Th are usually considered to have almost the same degree of incompatibility relative to partial melting (*Lemarchand* et al., 1987; *Sun* and *McDonough*, 1989, and references therein). Therefore a ratio of their distribution coefficients (D_{Ta}/D_{Th}) of about 10 during

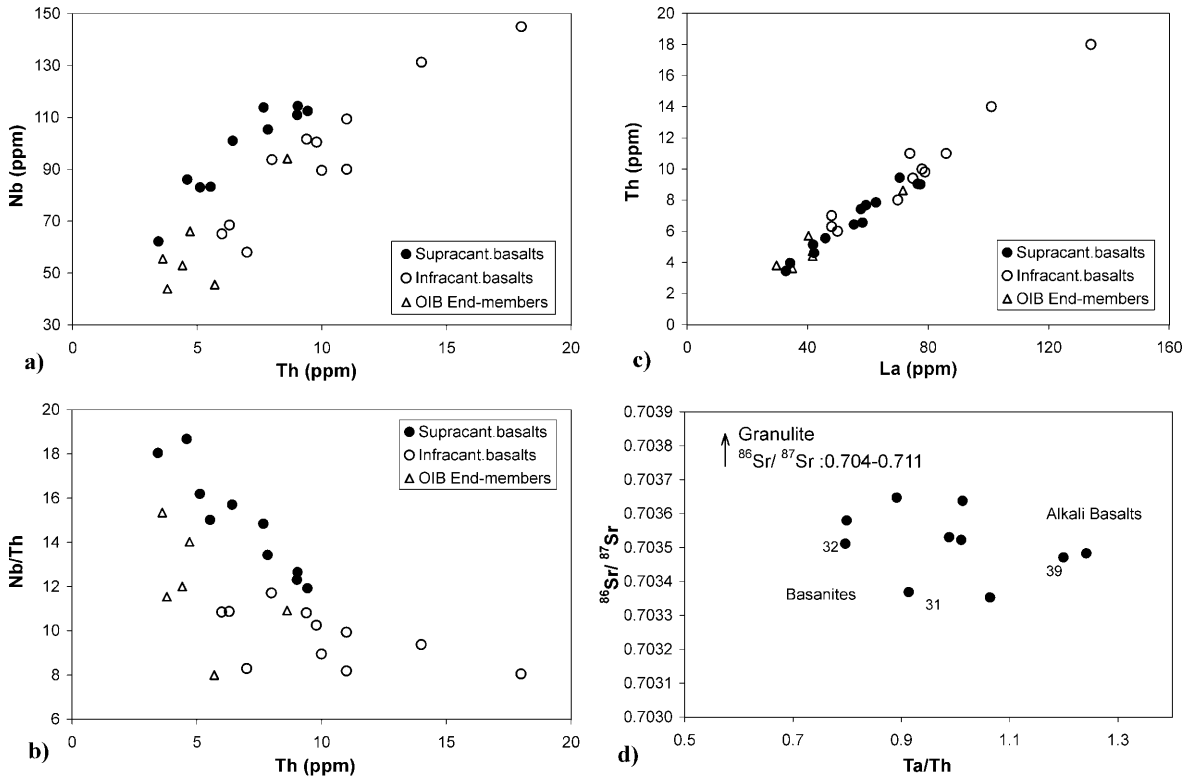

Fig. 7. OIB end-members composition from a compilation of *Wedepohl* and *Baumann* (1999). **a** Nb vs Th diagram for Supracantalian and Infracantalian basalts. **b** Nb–Th ratio vs Th diagram for Supracantalian and Infracantalian Basalts. **c** La vs Th diagram for Supracantalian and Infracantalian Basalts. **d** $^{86}Sr/^{87}Sr$ isotopic ratio vs Ta–Th ratio diagram for Supracantalian basalts. Granulite composition from *Downes* et al. (1986)

melting of a normal mantle seems too high. This assumption is supported by the fact that a Nb/Th ratio ranging from 8 to 19, as present in the Cantal basalts (Fig. 7b), has never been observed in any oceanic island (*Bodinier*, written communication). In conclusion, the variation of the Ta/Th ratio from basanites to basalts cannot be explained by a variation of the degree of partial melting of a normal mantle.

Crustal contamination

According to *Downes* and *Leyreloup* (1986), the granulitic crust in the Massif Central has a $^{87}Sr/^{86}Sr$ ratio of between 0.704 and 0.711. Basalts and basanites are characterized by low $^{87}Sr/^{86}Sr$ ratios (0.70335–0.70358). In order to explain the decrease of the Ta/Th ratio from basalts to basanites by crustal assimilation, a correlation between the Sr isotope ratios and the Ta/Th ratios has to be observed. However, no correlation has been found between $^{87}Sr/^{86}Sr$ and the Ta/Th ratio (Fig. 7d). Crustal contamination can therefore be excluded as an explanation of the decrease of the Ta/Th from basalts to basanites. Furthermore, *Wilson* et al. (1995) indicate the lack of crustal contamination in the mafic rocks of the Cantal massif.

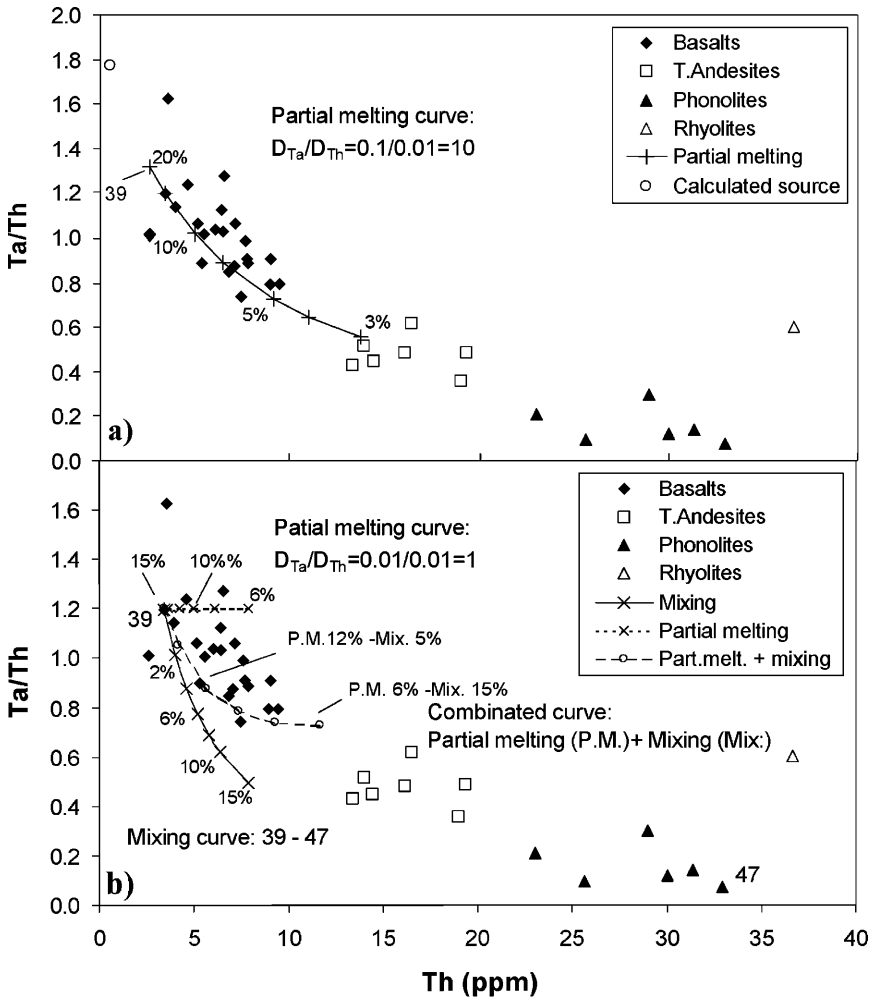

Fig. 8. **a** Ta–Th ratio vs Th diagram for Supracantalian rocks. Batch melting curve calculated with $D_{Th} = 0.01$ and $D_{Ta} = 0.1$. Hypothesis: basalt 39 corresponding to $F = 0.15$. **b** Ta–Th ratio vs Th diagram for Supracantalian rocks. Mixing curve calculated between the alkali basalt 39 and the phonolite 47. Batch melting curve calculated with $D_{Th} = 0.01$ and $D_{Ta} = 0.01$. Combined curve calculated with a rate of mixing of 15% for the composition corresponding to 6% of partial melting

Mixing with a second component

As already shown, the presence of GCPX pyroxenes in Supracantalian basalts and basanites indicates possible mixing between basaltic and phonolitic liquids. If phonolites are derived from the fractional crystallization of basalts, their very low Ta/Th ratio (0.3 to 0.06) can be explained by the fractional crystallization of magnetite, ilmenite and titanite, with Ta becoming increasingly compatible for more differentiated liquids (*Villemant* et al., 1981; *Lemarchand* et al., 1987). A calculated mixing curve between an alkali basalt (sample 39) and a phonolite (sample 47) does not fit the data (Fig. 8b).

If this mixing process is associated with a variation of the degree of partial melting assuming $D_{Ta}/D_{Th} = 1$, it should be possible to construct a combined

curve (Fig. 8b) to explain the decrease of the Ta/Th ratio from alkali basalts to basanites.

In that case, however, a strange and unrealistic inverse correlation appears between the degree of partial melting and the percentage of mixing. To explain the evolution of the Ta/Th ratios, the rocks resulting from the lowest degree of partial melting would be correlated with the higher degree of mixing and vice versa.

Discussion

Mixing or metasomatism

The presence of GCPX in basalts and basanites is consistent with the mixing process invoked to explain the Ta/Th ratio decrease from basalts to basanites. However, this model fails to explain two facts:

(i) the enrichment of Ta and Nb in the Supracantalian rocks compared with the Infracantalian basalts, and (ii) the fact that the mixing process seems inversely proportional to the degree of partial melting.

Whereas all earlier hypotheses assume a normal mantle composition, *Clague* and *Frey* (1982) have suggested that the presence of titanate minerals in the mantle could influence the Ta, Nb, Zr, Ti and Hf contents in basaltic melts. *Bodinier* et al. (1996) and *Bedini* et al. (1999) subsequently demonstrated the presence of these minerals in peridotites from the Ronda massif (Spain) and the East African Rift (Ethiopia). Titanates consist of a very thin reaction layer ($<10\,\mu m$ thick) coating the surface of spinels, which essentially concentrate Ta and Nb. According to *Bodinier* et al. (1996), these spinel coatings result from a metasomatic process involving the percolation of small silica-rich and K-rich melt fractions in the lithospheric mantle.

By adding 0.01% of the rutile component shown to exist by *Bodinier* et al. (1996) to a spinel of peridotite composition, an increase of the Ta content from 0.037 (primitive mantle composition; *McDonough*, 1998) to 0.365 ppm is obtained. Similarly, the Ta/Th ratio increases from 0.46 (primitive mantle ratio) to 4.56 in the metasomatized peridotite. A similar calculation based on Ti contents shows an enrichment from the primitive mantle composition (1200 ppm, *McDonough*, 1998) to 1250 ppm. This Ti enrichment is too low to be observed in the basaltic compositions after partial melting of the metasomatized mantle source. The partial melting of a mantle source containing 0.01% of titanate minerals could explain the high Ta/Th ratio observed in the Cantal basalts. Furthermore, the addition of compatible Ta–Nb-bearing phases to a peridotite will change the degree of incompatibility of these elements during partial melting. *Bodinier* et al. (1996) calculated that the bulk coefficients of Ta and Nb for such a peridotite increase by a factor of 10. A calculated curve for partial melting with a ratio of $D_{Ta}/D_{Th} = 0.1/0.01 = 10$ (Fig. 8a) shows that a variation in the degree of partial melting of such a metasomatized source could explain the decrease in the Ta/Th ratio from basalts to basanites.

In conclusion, two mechanisms could explain the Ta/Th variation:

– Mixing between a basaltic and a phonolitic liquid, as demonstrated by the presence of GCPX clinopyroxene in basalts and basanites. Taking into account the absence of a clear mixing trend for the major elements between basalts and

phonolites, our calculations show that the proportion of phonolitic liquid in the mixing needs to be lower than 2%.
– Percolation of Si and K-rich melt across the lithospheric mantle leading to the formation of a Ta–Nb-rich oxide layer in the mantle. This metasomatism could explain the high Ta and Nb content of the mantle source on the one hand and the correlative decrease of the Ta/Th ratio and the degree of partial melting on the other hand.

When did the metasomatic event occur?

The Infracantalian basalts show about the same range of composition as the Supracantalian basalts (Figs. 1 and 6). However, a difference appears between these two basalts as regards their enrichment in Nb, Ta and the change of their degree of incompatibility in the Supracantalian lavas (Figs. 7a and 7b). If partial melting of an OIB source could explain the Ta, Nb contents of the Infracantalian rocks (Fig. 7a), the presence of Ta–Nb-rich oxides in the source of the Supracantalian basalts is necessary in order to explain their high Ta and Nb contents and the decrease of incompatibility for Ta and Nb in these rocks.

A possible hypothesis to explain the absence or presence of Ta, Nb-rich oxides in the Infra- and Supracantalian basalt sources respectively could be their occurrence at a particular depth in the mantle. In this case, the differences between the Infra and Supracantalian basalts could be connected to the variation of the depth of partial melting. However *Albarède* (1992) showed that the MgO and SiO_2 contents are correlated with the pressure conditions during the melting event. Thus, the similarity of MgO, SiO_2 and other major element contents in the two groups of basalts (Table 2) leads us to exclude this hypothesis. The similarity between the Infra and Supracantalian basalts seems to suggest that the addition of Ta, Nb-rich oxides took place in the same mantle source during the time interval between the deposition of the Infracantalian basalts (13–9.5 Ma) and the Supracantalian basalts (9.5–2 Ma). If this assumption is correct, this difference constitutes a major premise because, in this case, the metasomatic event necessarily occurred between the two stages of basalt deposition and could be related to the Tertiary volcanic activity but not to older (e.g. Variscan) events.

Is there a relationship between mantle metasomatism and formation of GCPX?

Almost all the Supracantalian basalts contain GCPX whereas most of the Infracantalian basalts do not. As already mentioned, the presence of composite cores (Plate 1, photograph 4) in a 9–10 Ma basaltic lava clearly suggests the existence of batches of phonolitic liquid at depth at around ~ 10 Ma. The inferred temporal association of phonolitic melts and percolation of a potential metasomatic melt suggest a link between the formation of the green pyroxenes and the metasomatic mantle processes.

In order to explain the formation of a thin Nb–Ta-rich reaction layer coating the surface of spinels in mantle peridotites, *Bodinier* et al. (1996) suggested the percolation of small silica-rich and K-rich melt fractions in the lithospheric mantle.

Their estimated compositions are close to those of phonolitic melts within which the GCPX pyroxenes could crystallize. *Aspen* et al. (1990) and more recently *Upton* et al. (1999) described Nb-rich oxides associated with Fe–Na augites in some mantle xenoliths of the Scottish volcanic province. These occurrences suggest that both mineral assemblages may coexist under similar physical and chemical conditions. *Schiano* and *Clocchiatti* (1994) as well as *Coltorti* et al. (1999 and references therein) describe numerous occurrences of small melt fractions trapped in peridotite from alkali basaltic provinces which display a wide range of chemical compositions from basalts to trachytes and phonolites. The origin of these melts is currently a matter of debate, but any such process requires a metasomatic event in the upper mantle.

From their study of veined xenoliths on La Palma (Canary Islands), *Wulff-Pedersen* et al. (1999) concluded that small alkali-Si-rich melt fractions may result from in-situ reactions between basaltic magma percolating through the mantle peridotite. These basaltic melts occur as amphibole-rich veins consisting of kaersutite, augite, olivine, Fe–Ti-oxide, phlogopite, traces of apatite, brownish basaltic glass and in some cases hauyne. *Neumann* and *Wulff-Pedersen* (1997) called this process Infiltration-Reaction-Crystallization (IRC). These authors concluded that IRC may represent the general mode of formation of highly silicic melts in the upper mantle, which may represent an important metasomatic agent.

Wulff-Pedersen et al. (1999) also described Nb-rich Fe–Ti oxides in these amphibole veins. These oxides may represent the source of the Nb–Ta enrichment of the mantle through the formation of thin oxide layers at the surface of spinels. Moreover, the augites included within amphibole veins (*Wulff-Pedersen* et al., 1999) have a composition close to that of the GCPX from Cantal basalts (Table 1, Figs. 3 and 4). This feature suggests that these GCPX may have crystallized from basaltic melt percolating through the upper mantle. In the Cantal massif, we observed the association of GCPX with feldspar (Oligoclase An_{20-30}). This association indicates an evolved melt composition, an observation which contradicts the basaltic composition of percolating melts suggested by *Wulff-Pedersen*. Furthermore, *Upton* et al. (1999) interpreted the association of anorthoclase, Fe-rich biotite, Na–Fe salite, kaersutite, apatite, oxides, etc. in alkali basalts of Scotland as the crystallization products of salic alkaline magmas within the upper mantle and/or within ultramafic rocks from the lowermost crust. All these data suggest an evolved composition for the liquid in which our GCPX crystallized.

Bedini et al. (1997, 1999) described a compositional variation of pervasively infiltrated melts which metasomatized the lithosphere below the East African Rift. These authors suggest that the upward migration of the percolation front would be associated with continuous crystallization of small melt fractions and with the formation of Ta–Nb-rich oxide layers as well as the deposition of apatite and clinopyroxene in the peridotites. The variation of trace element contents from deeper recrystallized peridotite, with only slight enrichments in LILE, to higher less recrystallized peridotite, with a high LILE content and a negative HFSE anomaly (Nb, Ta, Zr, Hf and Ti), implies an evolution of the percolating liquids. A similar process known as ''percolative fractional crystallization'', is suggested by *Harte* et al. (1993) to explain the chemical evolution of metasomatic melts in mantle rocks. This mechanism would account for the evolution of alkali

basaltic or basanitic melts towards evolved liquids during percolation within the mantle.

On the basis of the basaltic nature of the percolative melts proposed in the IRC process, the IRC model alone seems unable to account for all the previous observations. We thus propose a model associating the IRC process with the ''percolative fractional crystallization'' hypothesis, that could explain: i) the formation of small Si-rich melt fractions in the mantle, ii) the chemical evolution of the metasomatic fluid in the lithospheric mantle, and iii) the temporal connection between precursor melts of the volcanic activity and metasomatic events observed in some regions (*Bedini* et al., 1997; this work). The recent description (*Lenoir* et al., 2001) of a melting process related to the rise of a thermal front in Ronda peridotite supports the same idea. These authors documented a process of partial melting followed by a melt migration by porous flow on a kilometer scale. This migration is associated with the deposition of Ta–Nb-rich oxides in the mantle and seems to correspond to the beginning of the percolative fractional crystallization process.

According to this model, GCPX would crystallize within the latest melts of phonolitic composition formed by percolative fractional crystallization. The compositional evolution of the percolative melts in which GCPX crystallize is in agreement with the wide compositional range of GCPX. Ta–Nb-rich oxide coatings could be associated with a higher level in the percolative-reaction front (*Bedini* et al., 1997). This model implies the deposition of accessory phases in the lithospheric mantle and the removal of these phases during the formation of the Supracantalian basalts.

Conclusion

The enrichment in Ta and Nb in the Supracantalian basalts appears to be related to the percolation of metasomatic liquids through the mantle associated with the deposition of Ta–Nb-rich oxides during or just before the deposition of late Miocene volcanic products. These metasomatic accessory phases are removed with the formation of the Supracantalian basalts.

The appearance of GCPX in the basalts at this time suggests a relationship between their crystallization and the metasomatic event. Because of the similarity in composition between the GCPX and the pyroxene of phonolites and its association with oligoclase An_{20}, we suggest that the chemical composition of the metasomatic liquids was close to that of the phonolitic liquids. One argument in favor of this relationship is the recent discovery of pyroxene of similar composition to GCPX in metasomatized peridotites (*Wulff-Pedersen* et al., 1999). The timing of the deposition of Ta–Nb-rich oxides just before or during the deposition of the Infracantalian basalts clearly indicates that the metasomatic process is produced by the magmatic activity itself, which is related to an asthenospheric upwelling.

We suggest that a combination of the IRC process (*Wulff-Pedersen* et al., 1999) and the ''fractional percolative crystallization'' model of *Harte* et al. (1993) and *Bedini* et al. (1997) could produce a compositional range of this kind. Hence, the actual range might be much larger than that of the basaltic compositions estimated by *Wulff-Pedersen* et al. (1999) for metasomatic liquids in Canary Island peridotites.

Finally, GCPX are described in most continental alkali basaltic provinces (Tertiary European volcanic province, North Africa, Australia) as well as in some oceanic islands (Isla da Trinidade, Tristan da Cunha, Canary Islands). Their wide occurrence provides evidence for a ''general process'' linked to the origin and evolution of the alkaline series. Their presence in these series would be linked directly to a specific mode of metasomatism in the mantle beneath some alkali provinces.

Acknowledgments

The invaluable help of *F. Bussy* during the microprobe analyses and his contribution in daily discussions is highly appreciated. Thanks are also due to all members of the ''Friday workshops'' for their active discussions on GCPX. Special thanks go to *A. Collomb*, who moved on to a hydrogeology project after the first part of this work; she will always be part of our staff. This work benefited from discussions with the participants of the meeting organized by *P. Nehlig* in Aurillac (1999) as well as from those held with the participants of the ''3ème Journée Magmatique'' which took place in Lausanne in 1999. Thanks are also due to *J.-Ph. Eissen* for his support during the writing of this paper. We also wish to express our warm acknowledgements to *J.L. Bodinier* and *R. Maury* for their constructive reviews which greatly improved the presentation of the data. We thank *F. Bussy* and *A. Mulch* for their help in improving the English version of this paper.

The P. Süe laboratory (Saclay, France) supported our INAA analyses. The help of *D. Fontigny* (Geneva) and *J. Kramers* (Bern) during the isotopic analyses is acknowledged with gratitude. The Wilhelm Friedländer Stiftung contributed to the field work of *J. Hernandez. S. Pilet* benefited from a grant of the University of Lausanne.

References

Albarède F (1992) How deep do common basaltic magmas form and differentiate? J Geophys Res B97: 10,997–11,009

Allègre CJ, Schiano P, Lewin E (1995) Differences between oceanic basalts by multitrace element ratio topology. Earth Planet Sci Lett 129: 1–12

Aspen P, Upton BGJ, Dickin AP (1990) Anorthoclase, sanidine and associated megacrysts in Scottish alkali basalts; high-pressure syenitic debris from upper mantle sources? Eur J Mineral 2: 503–517

Bakkine J, Conquéré F, Vilminot JC (1968) Les caractères particuliers du volcanisme au Nord de Montpellier: l'absarokite du Pouget; la ferrisalite sodique de Gabels. Bull Soc Fr Minéral Cristallogr 91: 141–150

Barton M, Van Bergen MJ (1981) Green clinopyroxenes and associated phases in a potassium-rich-lava from the Leucite Hills, Wyoming. Contrib Mineral Petrol 77: 101–114

Barton M, Varekamp JC, Van Bergen MJ (1982) Complex zoning of clinopyroxenes in the lavas of Vulsini, Latium, Italy; evidence for magma mixing. J Volcanol Geotherm Res 14: 361–388

Bedini RM, Bodinier JL (1999) Distribution of incompatible trace elements between the constituents of spinel peridotite xenoliths; ICP-MS data from the East African Rift. Geochim Cosmochim Acta 63: 3883–3900

Bedini RM, Bodinier JL, Dautria JM, Morten L (1997) Evolution of LILE-enriched small melt fractions in the lithospheric mantle; a case study from the East African Rift. Earth Planet Sci Lett 153: 67–83

Bodinier JL, Merlet C, Bedini RM, Simien F, Remaidi M, Garrido CJ (1996) Distribution of niobium, tantalum, and other highly incompatible trace elements in the lithospheric mantle; the spinel paradox. Geochim Cosmochim Acta 60: 545–550

Bourdier J, De Goer DHA, Rançon JP, Vincent PM (1989) Large debris-avalanche deposits on the south and west flanks of the Cantal Massif; stratigraphic and volcano-structural implications. Compt Rend Acad Sci Paris 309: 2127–2133

Brousse R, Maury RC, Clocchiatti R (1979) Volcanism of Mont-Dore. In: *Brousse R, Wimmenauer W* (eds) Alkalic volcanism connected to Cenozoic distensions of Western Europe: the Central Massif, Rhine Graben; guidebook. Sciences de la Terre 23: 48–50

Cantagrel JM (1995) Debris avalanches and debris flows in a complex intraplate volcano; towards a new volcano-structural scheme for the Cantal Massif, Central Massif, France. Bull Soc Géol France 166: 285–293

Chauvel C, Hofmann AW, Vidal P (1992) HIMU-EM; the French Polynesian connection. Earth Planet Sci Lett 110: 99–119

Civetta L, Innocenti F, Lirer L, Manetti P, Munno R, Peccerillo A, Poli G, Serri G (1979) Potassic and highly potassic series of Ernic Mountains, southern Latium; petrologic and geochemical considerations. Rend Soc Ital Mineral Petrol 35: 227–249

Clague DA, Frey FA (1982) Petrology and trace element geochemistry of the Honolulu Volcanics, Oahu; implications for the oceanic mantle below Hawaii. J Petrol 23: 447–504

Collomb A, Pilet S (1996) Pétrologie et minéralogie de la zone centrale du massif volcanique du Cantal (Massif central, France): évolution par cristallisation fractionnée; origine des pyroxènes verts des basaltes alcalins. Thesis, Université de Lausanne, 189 pp

Coltorti M, Bonadiman C, Hinton RW, Siena F, Upton BGJ (1999) Carbonatite metasomatism of the oceanic upper mantle; evidence from clinopyroxenes and glasses in ultramafic xenoliths of Grande Comore, Indian Ocean. J Petrol 40: 133–165

Dobosi G, Fodor RV (1992) Magma fractionation, replenishment, and mixing as inferred from green-core clinopyroxenes in Pliocene basanite, southern Slovakia. Lithos 28: 133–150

Downes H (1984) Sr and Nd isotope geochemistry of coexisting alkaline magma series, Cantal, massif Central, France. Earth Planet Sci Lett 69: 321–334

Downes H, Leyreloup A (1986) Granulitic xenoliths from the French Massif Central; petrology, Sr and Nd isotope systematics and model age estimates. Geol Soc Lond, Spec Publ 24: 319–330

Duda A, Schmincke HU (1985) Polybaric differentiation of alkali basaltic magmas; evidence from green-core clinopyroxenes (Eifel, FRG). Contrib Mineral Petrol 91: 340–353

Frisch T, Schmincke HU (1970) Petrology of clinopyroxene-amphibole inclusions from the Roque Nublo volcanics, Gran Canaria, Canary islands. Petrology of Roque Nublo volcanics, I. Bull Volcanol 33: 1073–1088

Glangeaud L, Letolle R (1966) The two-magma theory in intracontinental volcanism and the geochemical evolution of the Mont-Dore lavas, France. Geol Rundsch 55: 316–329

Greenwood JC (1998) Barian-titanian micas from Ilha da Trinidade, South Atlantic. In: *Redfern SAT* (ed) Equilibrium and kinetic properties of minerals. Mineral Soc 62: 687–695

Harte B, Hunter RH, Kinny PD (1993) Melt geometry, movement and crystallization, in relation to mantle dykes, veins and metasomatism. Phil Trans Roy Soc Lond A342: 1–21

Hemond C, Devey CW, Chauvel C (1994) Source compositions and melting processes in the Society and Austral plumes (South Pacific Ocean); element and isotope (Sr, Nd, Pb, Th) geochemistry. Chem Geol 115: 7–45

Hernandez J (1971) Le volcanisme tertiaire des monts du Forez et de la plaine de Montbrison. Thèse 3e cycle, Paris VI, 129 pp

Hernandez J (1973) Le volcanisme tertiaire des monts du Forez (Massif central français): basanites à analcime, à leucite et néphélinites à mélilite. Bull Soc Fr Minéral Cristallogr 96: 303–312

Huckenholz HG (1966) The petrogenetic evolution of clinopyroxenes in Tertiary volcanics of the Hocheifel, III. The clinopyroxenes of picrite basalts (ankaramites). Contrib Mineral Petrol 12: 73–95

Ibhi A (2000) Etude pétrologique et minéralogique des roches alcalines néogène-quaternaire de Jbel Saghro et de leurs enclaves associées (Anti-atlas, Maroc). Thesis, Université Ibnou Zohr, Agadir, Maroc, 321 pp

Jung J, Brousse R (1962) Les provinces volcaniques néogènes et quaternaires de la France. Bull Serv Carte Géol France 267: 569–629

Le Maitre RW (1989) A classification of igneous rocks and glossary of terms: Recommendations of the International Union of Geological Sciences Subcommision on the systematics of igneous rocks. Blackwell, Oxford, 193 pp

Lemarchand F, Villemant B, Calas G (1987) Trace element distribution coefficients in alkaline series. Geochim Cosmochim Acta 51: 1071–1081

Lenoir X, Garrido CJ, Bodinier JL, Dautria JM, Gervilla F (2001) The recrystallization front of the Ronda Peridotite; evidence for melting and thermal erosion of subcontinental lithospheric mantle beneath the Alboran Basin. J Petrol 42: 141–158

Liotard JM, Briqueu L, Dautria JM, Jakni B (1999) Basanites and nephelinites from Bas-Languedoc; mantle heterogeneities and crustal contamination. Bull Soc Géol France 170: 423–433

Lloyd FE (1981) Upper-mantle metasomatism beneath a continental rift; clinopyroxenes in alkali mafic lavas and nodules from South West Uganda. Mineral Mag 44: 315–323

Maury R (1976) Contamination et cristallisation fractionnée de séries volcaniques alcalines continentales (Massif Central français) et océaniques (Pacifique Central): origine des laves acides. Thesis, Université de Paris XI

Maury RC, Varet J (1980) Tertiary and Quaternary volcanism in France. In: Evolutions géologiques de la France, Vol 107. Bureau de Recherches Géologiques et Minières (BRGM), pp 137–159

Maury RC, Brousse R, Villemant B, Joron JL, Jaffrezic H, Treuil M (1980) Fractional crystallization of an alkali basalt magma: the Chaine des Puys volcanic series, Central Massif, France. I. Petrology. Bull Minéral 103: 250–266

McDonough W (1998) Earth's Core. In: The encyclopedia of geochemistry. Chapman and Hall (http://earthref.org/GERM/)

Morimoto N, Fabries J, Ferguson AK, Ginzburg IV, Ross M, Seifert FA, Zussman J, Aoki K, Gottardi G (1988) Nomenclature of pyroxenes. Am Mineral 73: 1123–1133

Nehlig P, Leyrit H, Dardon A, Freour G, de Goer de Herve A, Huguet D, Thieblemont D (2001) Constructions et destructions du stratovolcan du Cantal. Bull Soc Geol France 172; 3: 295–308

Neumann ER, Wulff-Pedersen E (1997) The origin of highly silicic glass in mantle xenoliths from the Canary Islands. J Petrol 38: 1513–1539

Nimis P (1999) Clinopyroxene geobarometry of magmatic rocks, part 2. Structural geobarometers for basic to acid, tholeiitic and mildly alkaline magmatic systems. Contrib Mineral Petrol 135: 62–74

Perrier G, Ruegg JC (1974) Structure of the crust and upper mantle in the French Central Massif. Eos 55: 359–360

Platevoet R, Schneider JL, Lef èvre C, Nehlig P (1999) Les formations pyroclastiques du strato-volcan du Cantal sont-elles liées à une vaste caldéra centrale? Apport des dynamismes volcaniques. Géol France 4: 77–91

Rachdi HEN, Velde D, Hernandez J (1995) L'association volcanique plio-quaternaire basanite–nephelinite–phonolite du Maroc Central (translated title: The Plio-Quaternary basanite nephelinite phonolite association from central Morocco). Compt Rend Acad Sci Paris 301: 1293–1298

Reubi O, Hernandez J (2000) Volcanic débris avalanche deposits of the upper Maronne valley (Cantal volcano, France): evidence for contrasted formation and transport mechanisms. J Volcanol Geotherm Res 102: 271–286

Schiano P, Clocchiatti R (1994) Worldwide occurrence of silica-rich melts in subcontinental and sub-oceanic mantle minerals. Nature 368: 621–624

Schneider JL, Fischer RV (1998) Transport and emplacement mechanisms of large volcanic debris avalanches: evidence from the northwest sector of Cantal Volcano (France). J Volcanol Geotherm Res 83: 141–165

Sun SS, McDonough WF (1989) Chemical and isotopic systematics of oceanic basalts; implications for mantle composition and processes. Geol Soc Lond, Spec Publ 42: 313–345

Thompson RN (1974) Some high-pressure pyroxenes. Mineral Mag 39: 768–787

Upton BGJ, Hinton RW, Aspen P, Finch AA, Valley JW (1999) Megacrysts and associated xenoliths; evidence for migration of geochemically enriched melts in the upper mantle beneath Scotland. J Petrol 40: 935–956

Villemant B (1985) La différentiation des séries volcaniques: géochimie des éléments traces dans les séries du Massif Central et d'ltalie Centrale. Thesis, Université Pierre et Marie Curie

Villemant B, Joron JL, Jaffrezic H, Treuil M, Maury R, Brousse R (1980) Fractional crystallization of an alkali basalt magma; the Chaine des Puys volcanic series, Central Massif, France. II. Geochemistry. Bull Minéral 103: 267–286

Villemant B, Jaffrezic H, Joron JL, Treuil M (1981) Distribution coefficients of major and trace elements; fractional crystallization in the alkali basalt series of Chaine des Puys (Massif Central, France). Geochim Cosmochim Acta 45: 1997–2016

Wass SY (1979) Multiple origins of clinopyroxenes in alkali basaltic rocks. Lithos 12: 115–132

Wedepohl KH, Baumann A (1999) Central European Cenozoic plume volcanism with OIB characteristics and indications of a lower mantle source. Contrib Mineral Petrol 136: 225–239

Wilson M, Downes H (1991) Tertiary-Quaternary extension-related alkaline magmatism in Western and Central Europe. J Petrol 32: 811–849

Wilson M, Downes H, Cebria JM (1995) Contrasting fractionation trends in coexisting continental alkaline magmas series; Cantal, Massif Central, France. J Petrol 36: 1729–1753

Wulff-Pedersen E, Neumann ER, Vannucci R, Bottazzi P, Ottolini L (1999) Silicic melts produced by reaction between peridotite and infiltrating basaltic melts: ion probe data on glasses minerals in veined xenoliths from La Palma, Canary Islands. Contrib Mineral Petrol 137: 59–82

Authors' address: Dr. *J. Hernandez*, Institute of Mineralogy and Geochemistry, University of Lausanne, BFSH2, CH-1015 Lausanne, Switzerland, e-mail: jean.hernandez@img.unil.ch